CrossMark

ORIGINAL PAPER: SOL-GEL AND HYBRID MATERIALS FOR DIELECTRIC, ELECTRONIC, MAGNETIC AND FERROELECTRIC APPLICATIONS

Preparation and microwave absorbing properties of polyaniline/NiFe$_2$O$_4$/graphite nanosheet composites via sol–gel reaction and in situ polymerization

Xingliang Chen[1] · Shuhua Qi[1]

Abstract Excellent microwave absorption of polyaniline composites with NiFe$_2$O$_4$/graphite nanosheet was prepared via sol–gel method and in situ polymerization reaction. The obtained composites were characterized by scanning electron microscopy, transmission electron microscopy, X-ray diffraction, thermogravimetric analyzer, vibrating sample magnetometer and a vector network analyzer. The results indicated that the graphite nanosheet was completely covered by NiFe$_2$O$_4$ particles and NiFe$_2$O$_4$/ graphite nanosheet is wrapped by polyaniline. Polyaniline /NiFe$_2$O$_4$/ graphite nanosheet has better thermal stability than polyaniline, and its conductivity and Ms are 0.2 S/cm and 10 emu/g, respectively. Measurement of the vector network analyzer indicates that the microwave absorbing properties of polyaniline /NiFe$_2$O$_4$/ graphite nanosheet are better than those of graphite nanosheet, NiFe$_2$O$_4$, polyaniline and polyaniline / graphite nanosheet. Its maximum reflection loss value is −21 dB at 11.5 GHz when the thickness is 2.0 mm, and polyaniline /NiFe$_2$O$_4$/ graphite nanosheet's best match thickness is 2.5 mm, its reflection loss value can reach −30 dB at 9.1 GHz in the X band.

Graphical Abstract
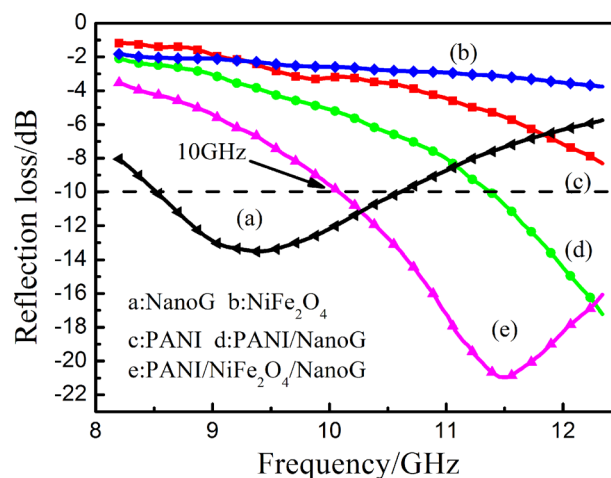
a:NanoG b:NiFe$_2$O$_4$
c:PANI d:PANI/NanoG
e:PANI/NiFe$_2$O$_4$/NanoG

✉ Shuhua Qi
qishuhuanwpu@163.com

1 Department of Applied Chemistry, School of Natural and Applied Sciences, Northwestern Polytechnical University, Xi'an 710072 Shaanxi, China

1 Introduction

With the advancement of modern science and technology, microwave absorption materials have played an important role in our society for its special functions. For instance, in the application of high power radar, communication equipment, microwave heating device, absorbing material can prevent leakage of electromagnetic radiation and protect the health of the operator. Meanwhile, with a growing

importance in stealth technology and electromagnetic compatibility (EMC), electromagnetic wave absorbing material also has an outstanding role. So absorbing materials with light weight, broad frequency and strong absorption peak become the focus of current research. Generally, microwave absorption materials are divided into two types on their different mechanism: electronic materials such as graphite nanosheet (NanoG) and magnetic materials such as ferrite [1–3]. When the conductive materials were combined with magnetic materials, perfect microwave absorbing materials with electrical conductivity and magnetic properties can be prepared [4–6].

Ferrite is a traditional microwave absorbing material with high saturation magnetization and magnetic loss, and has been widely applied in many fields such as military area and industrial. However, ferrite is a non-conductive material with very high density, which restricts its potential in applications requiring light mass and electrical conductivity. In order to prepare light-weight composites with efficiency microwave absorbing performance, carbon materials such as carbon nano-tube (CNT), carbon fiber (CF) and graphite nanosheet (NanoG) are always combined with ferrite [7–9]. Out of these materials, NanoG was choosen for its excellent electrical conductivity, cheap price, low density and other strengths [10].

Conductive polymers such as polyaniline (PANI), poly-pyrrole (PPY), poly thiophene (PHT) and polyacetylene (PAC) are popular research subjects for their special structures and properties. Conductive polymers are always used in the preparation of microwave absorbing composite materials [11–13]. As a conducting polymer, PANI has useful properties such as its cheap price, low weight and high conductivity, but its microwave absorbing property is low and frequency band is narrow [14]. To obtain perfect absorbing property, magnetic materials such as metal cobalt, metal nickel, ferrites and conductive materials such as carbon nano-tube, carbon fiber, graphene are always added to improve PANI's microwave absorbing property [15–17].

In this study, the expanded graphite was firstly stripped into nanometer size by ultrasonic treatment in ethanol solution to prepare the NanoG. Then, nickel ferrite ($NiFe_2O_4$)/NanoG composites were synthesized via sol–gel reaction, and the graphite nanosheet was coated by $NiFe_2O_4$. Then, homogeneous PANI/$NiFe_2O_4$/NanoG composites with low density and excellent absorption properties were prepared. The morphology structures of NanoG, $NiFe_2O_4$/NanoG, PANI and PANI/$NiFe_2O_4$/NanoG were examined by TEM, SEM and XRD. Other instruments such as four probes resistance tester, vibrating sample magnetometer, thermogravimetric analyzer and vector network analyzer were also used to characterize the reaction products.

2 Experimental

2.1 Preparation of NanoG

Graphite nanosheet was obtained from oxidized graphite (OG) via an uncomplicated two-step reaction. First, OG was subjected to a thermal expansion at 850–950 °C for about 15 s in a tube furnace to form expanded graphite (EG). Then EG was immersed in ethanol solution and stripped into nanometer size by ultrasonic treatment. Then, the product was filtered, rinsed with ethanol solution for several times and dried in a vacuum at 70 °C for about 12 h, finally the NanoG with nanometer size was successfully prepared.

2.2 Preparation of NiFe₂O₄/NanoG

$NiFe_2O_4$/NanoG was obtained by sol–gel reaction. Before the sol–gel reaction, the surface of NanoG was pretreated with KH550. $Ni(NO_3)_2$, $Fe(NO_3)_3$ (Fe/Ni ratio of 2) and the pretreated NanoG were mixed with the appropriate amount of $C_6H_8O_7$. The mixed components were ground until the fine mixture powder was obtained. Then, the mixture powder was put at 90 °C water bath and a small amount of $(CH_2OH)_2$ was dropwise into, the PH value was adjusted to 7–8 by adding $NH_3 \cdot H_2O$ solution, keeping the temperature for more than 2 h, until the solution became viscous and a gel was formed. The gel was then washed with deionized water several times to remove possible residues and dried at 65 °C for 10 h, then calcined at 700 °C (argon atmosphere) for 4 h. The reaction is shown in Fig. 1.

2.3 Synthesis of PANI/NiFe₂O₄/NanoG

The PANI/$NiFe_2O_4$/NanoG composite was prepared via in situ polymerization reaction, the process is shown in Fig. 1. 1.0 g $NiFe_2O_4$/NanoG was added into 30 ml HCl solution (0.5 mol l^{-1}), the mixture was then placed in an ice water bath and stirred. Then, 0.6 ml aniline was added into the mixture. When the temperature of the mixture was dropped to about 2–4 °C, 40 ml another solution was added
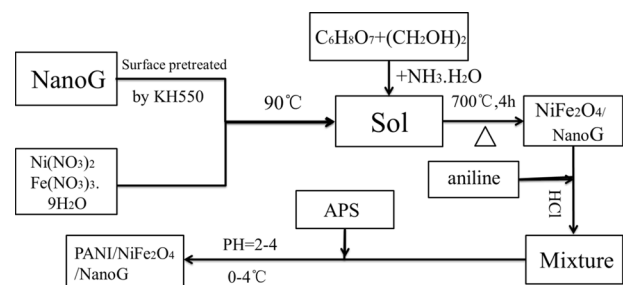

Fig. 1 Preparation of $NiFe_2O_4$/NanoG and PANI/$NiFe_2O_4$/NanoG

into the mixture, containing $(NH_4)_2S_2O_8$ (APS, 0.5 mol l^{-1}) and HCl (0.5 mol l^{-1}). The reaction was kept for 8 h. After the reaction, the reaction liquid was filtered, and washed several times with HCl solution, then the solid products were placed in a 90 °C vacuum for 6 h to obtain the PANI/$NiFe_2O_4$/NanoG.

2.4 Characterization

The structure of NanoG, $NiFe_2O_4$/NanoG, PANI and PANI/$NiFe_2O_4$/NanoG was characterized by scanning electron microscopy (SEM; JSM-6390, HITACHI, Japan) and X-ray diffraction (XRD; PANalytical, Holland). In addition, the $NiFe_2O_4$/NanoG and PANI/$NiFe_2O_4$/NanoG samples were observed by transmission electron microscopy (TEM, H-7650, HITACHI, Japan). The thermal stabilities were analyzed using a thermogravimetric analyzer (TGA, SDT-2960, USA) with a heating rate of 10 °C/min in the range from 40 to 800 °C under argon atmosphere. The electrical conductivities of compounds were measured by a SZ-82 digital four probes resistance tester (Suzhou Electronic Equipment Factory, China). For measurement of electrical properties, circle samples with a diameter of 15 mm and a thickness of 2 mm were prepared by casting them into stainless forms and cold-pressing them. The magnetic properties were measured using vibrating sample magnetometer (VSM, Lake Shore7307). The absorption properties of PANI, PANI/NanoG and PANI/ $NiFe_2O_4$/NanoG were analyzed using a vector network analyzer(Agilent technologies E8362B) in X-band, the samples were prepared using the mix of the products (20 wt%) and paraffin (80 wt%) in a mould with the size of $22.86 \times 10.16 \times 2$ mm.

3 Results and discussion

3.1 SEM/TEM analysis

The SEM and TEM images of the products are shown in Fig. 2. Figure 2a is the SEM image of NanoG, NanoG was lustrous, smooth and with uniform lamellar structure, its thickness is less than 100 nm, about 40–80 nm. Figure 2b is the SEM image of $NiFe_2O_4$/NanoG, it can clearly observed that the $NiFe_2O_4$ layer is well-distributed on the surface of NanoG. Figure 2c and d show the microcosmic appearance of PANI and PANI/$NiFe_2O_4$/NanoG, respectively. After the in situ polymerization, the surface of $NiFe_2O_4$/NanoG was completely covered by PANI. Figure 2e and f are the TEM images of $NiFe_2O_4$/NanoG and PANI/$NiFe_2O_4$/NanoG, which can further confirm the conclusions obtained by SEM
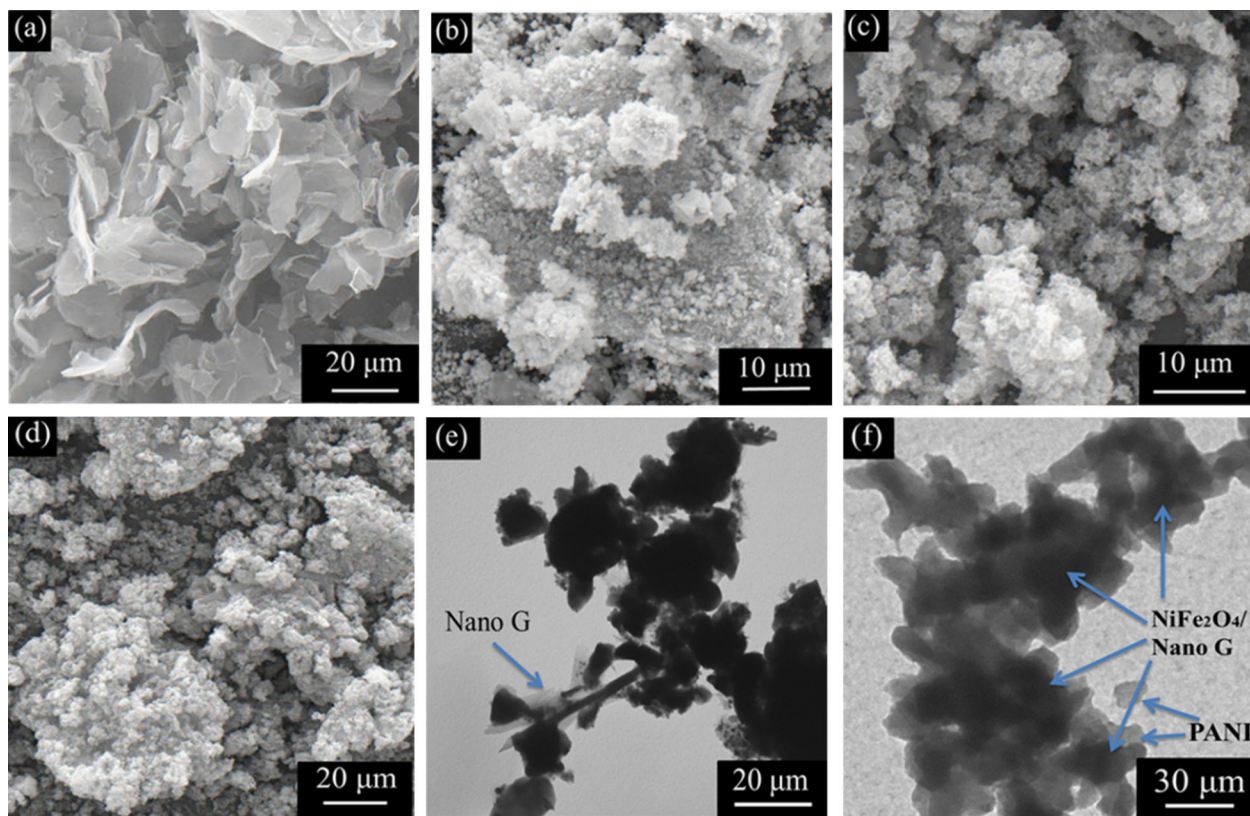

Fig. 2 SEM/TEM images of NanoG (a), $NiFe_2O_4$/NanoG (b, e), PANI (c) and PANI/$NiFe_2O_4$/NanoG (d, f)

images. These results indicate that the $NiFe_2O_4$/NanoG and PANI/$NiFe_2O_4$/NanoG are all successfully prepared.

3.2 XRD analysis

Figure 3 illustrates the XRD patterns of NanoG (a), $NiFe_2O_4$/NanoG (b), PANI (c) and PANI/$NiFe_2O_4$/NanoG from $2\theta = 10°$ to $80°$. The two peaks locate at $2\theta = 26.46°$ and $55.64°$ of curve (a), (b) and (d) are corresponding to (0 0 2) and (1 1 0) planes respectively and are the typical diffraction peaks of graphite (JCPDS. File No. 75-1621). Compare with curve (a), other six peaks can be observed at curve (b), which indicate the (220), (311), (400), (422), (511) and (440) planes of $NiFe_2O_4$'s cubic face-centered structure(JCPDS, File No. 10-0325). It suggests that the $NiFe_2O_4$/NanoG contains both $NiFe_2O_4$ and NanoG. The three peaks before $30°$ can easily be found at curve (c), which are the characteristic peaks of PANI. Figure 3d is the curve of PANI/$NiFe_2O_4$/NanoG, containing the characteristic peaks of PANI, $NiFe_2O_4$ and NanoG. These results confirm that $NiFe_2O_4$/NanoG and PANI/$NiFe_2O_4$/NanoG were both obtained.

3.3 TGA analysis

The thermal stability of material is an important property, which determines the temperature of the application of the material, so it is necessary to carry out thermal analysis. The thermal stabilities of PANI, PANI/NanoG and PANI/$NiFe_2O_4$/NanoG were characterized by TG analysis, and the curves are demonstrated in Fig. 4. The degradation temperature (T_d) of PANI is 511 °C for the pyrolysis of its main chain. Residual ratio (wt%) of PANI, PANI/NanoG and
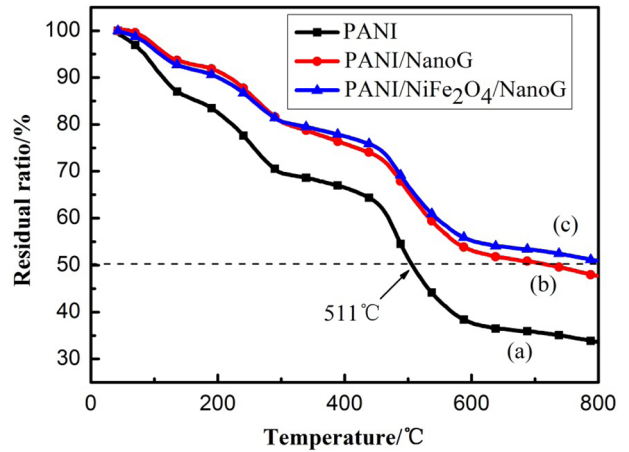

Fig. 4 TG curves of PANI (*a*) PANI/NanoG (*b*) and PANI/$NiFe_2O_4$/NanoG (*c*)

Table 1 Residual ratio (wt%) of PANI, PANI/NanoG and PANI/$NiFe_2O_4$/NanoG at different temperatures

Samples/Temperature	200 °C	400 °C	600 °C	800 °C
PANI	82.5	66.5	37.7	33.6
PANI/NanoG	91.3	75.5	53.2	47.8
PANI/$NiFe_2O_4$/NanoG	90.4	77.5	55.3	51.0

PANI/$NiFe_2O_4$/NanoG at different temperatures including 200, 400, 600 and 800 °C are shown in Table 1. Figure 4 and the table indicate that the PANI/NanoG's residual ratio and PANI/$NiFe_2O_4$/NanoG's residual ratio are relatively close at the four temperatures, while all the corresponding residual ratio values of the PANI are smaller than those of PANI/NanoG and PANI/$NiFe_2O_4$/NanoG. Meanwhile, the PANI's curve is lower than PANI/NanoG's curve and PANI/$NiFe_2O_4$/NanoG's curve. It can be attributed to the role of NanoG in imposing restriction on the pyrolysis of PANI chains and avoiding heat concentration [18].

3.4 Electrical conductivity

The conductivities of NanoG, $NiFe_2O_4$, $NiFe_2O_4$/NanoG, PANI, PANI/NanoG and PANI/$NiFe_2O_4$/NanoG are summarized in Tables 2 and 3. NanoG is an excellent conductive material with the high conductivity of 5.8 S/cm. The low conductivity of $NiFe_2O_4$ at 8.1×10^{-8} S/cm indicates that it is an insulating material. However, after the sol–gel reaction and combined with NanoG, the conductivity of $NiFe_2O_4$/NanoG can reach 0.24 S/cm, which can mainly attribute to the carbon material NanoG. As a conducting polymer, proton acid PANI has excellent conductivity, the four probes suggest that its conductivity can reach 0.19 S/cm. However, after adding the $NiFe_2O_4$/NanoG, its conductivity
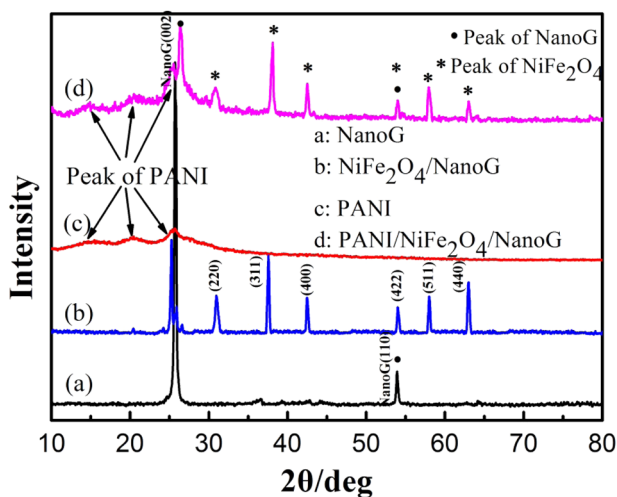

Fig. 3 XRD curves of NanoG (*a*) $NiFe_2O_4$/NanoG (*b*) PANI (*c*) and PANI/$NiFe_2O_4$/NanoG (*d*)

Table 2 Electrical conductivity values of NanoG, NiFe$_2$O$_4$, NiFe$_2$O$_4$/NanoG (S/cm)

Sample	NanoG	NiFe$_2$O$_4$	NiFe$_2$O$_4$/NanoG
Conductivity	5.8	8.1×10^{-8}	0.24

Table 3 Electrical conductivity values of PANI, PANI/NanoG and PANI/NiFe$_2$O$_4$/NanoG (S/cm)

Sample	PANI	PANI/NanoG	PANI/NiFe$_2$O$_4$/NanoG
Conductivity	0.19	1.6	0.2

Fig. 5 Magnetization curves of NiFe$_2$O$_4$ (*a*) NiFe$_2$O$_4$/NanoG (*b*) and PANI/NiFe$_2$O$_4$/NanoG (*c*)

increased to 0.2 S/cm, which is situated between the PANI's 0.19 S/cm and NiFe$_2$O$_4$/NanoG's 0.24 S/cm.

3.5 Magnetic performance

To verify the magnetic properties of the samples, the hysteresis loops were measured with VSM at room temperature, and the result was exhibited in Fig. 5. The hysteresis loops of the samples exhibit typical soft magnetic behavior. The magnetization saturation (Ms) of NiFe$_2$O$_4$ can reach 49.7 emu/g. After the sol–gel reaction and in situ polymerization, and being combined with nonmagnetic materials NanoG and PANI, its magnetism drops to 33 and 10 emu/g, respectively. It's mainly attributing to the contribution of the volumes of the non-magnetic NanoG and PANI to the total sample volume.
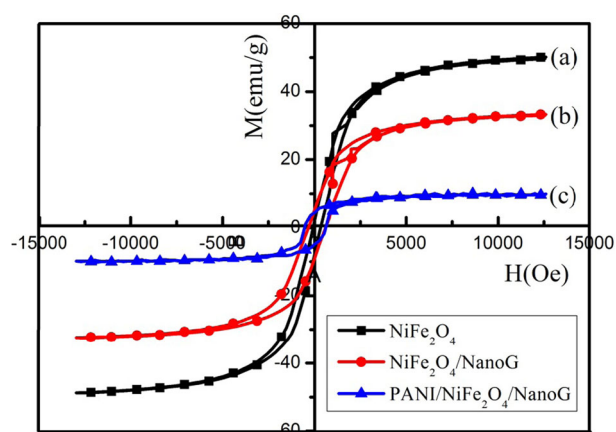
3.6 Microwave absorbing performance analysis

The mechanism of microwave energy loss in a material is the result of its magnetic and electronic properties, which is related to the complex permittivity and mainly characterized by reflection loss (RL). According to the transmit-line theory, when the electromagnetic wave vertically incidents upon the samples, the reflection loss can be calculated using the following equations [19–21]:

$$R = 20 \log \left| \frac{Z_{\text{in}} - Z_0}{Z_{\text{in}} + Z_0} \right| \tag{1}$$

$$Z_{\text{in}} = Z_0 \left(\sqrt{\frac{\mu_r}{\varepsilon_r}} \right) \tanh \left[j \left(\frac{2\pi f d}{c} \right) \left(\sqrt{\mu_r \varepsilon_r} \right) \right] \tag{2}$$

where Z_0 is the characteristic impedance of vacuum, Z_{in} is the normalized input impedance of the absorber, c is the velocity of light in free space, $\varepsilon_r = \varepsilon' - j\varepsilon''$, $\mu_r = \mu' - j\mu''$ is the relative complex permeability and permittivity of the material, f is the frequency, a is the velocity of the light, and d is the thickness of the absorber, respectively. It indicates that the absorption capacity of the material at the same

frequency mainly depends on the thickness of the material [22, 23].

The electromagnetic parameters of NanoG (a), NiFe$_2$O$_4$ (b), PANI (c), PANI/NanoG (d) and PANI/NiFe$_2$O$_4$/NanoG (e) were exhibited in Fig. 6, and their dielectric loss (tanδ_e = $\varepsilon''/\varepsilon'$) and magnetic loss (tan$\delta_m$ = μ''/μ') were calculated. The real permittivity (ε') and real permeability (μ') represent the storage ability of electromagnetic energy, and the imaginary permittivity (ε'') and imaginary permeability (μ'') are connected closely with the energy dissipation and magnetic loss, respectively. In the X band, the permittivities' real part of PANI, PANI/NanoG and PANI/NiFe$_2$O$_4$/NanoG are very close, all higher than NiFe$_2$O$_4$ and lower than NanoG. However, the permittivitie imaginary part of PANI/NiFe$_2$O$_4$/NanoG is higher than PANI/NanoG. Therefore, the PANI/NiFe$_2$O$_4$/NanoG's curve of tanδ_e is above those of PANI/Nano's and PANI's. In terms of magnetic parameters, due to the existence of the ferrite, all the parameters include μ', μ'' and tanδ_m of NiFe$_2$O$_4$ and PANI/NiFe$_2$O$_4$/NanoG are higher than PANI, NanoG and PANI/NanoG sample.

The calculated reflection loss curves of NanoG, NiFe$_2$O$_4$, PANI, PANI/NanoG and PANI/NiFe$_2$O$_4$/NanoG composite in X band are displayed in Fig. 7. The RL values of NiFe$_2$O$_4$ and PANI are all less than −10 dB (90 % absorption), which exhibit poor microwave absorbing property. The RL value of NanoG is ranging from −6 to −13 dB. After the sol–gel reaction and was combined with NanoG, the absorbing performance of PANI/NanoG was improved, and the maximum value of the reflection loss can reach −17.2 dB. However, the PANI/NiFe$_2$O$_4$/NanoG's curve is below the PANI/NanoG's curve and PANI's curve, and it can reach −21 dB (more than 99.9 % absorption) when the frequency is 11.5 GHz. In addition, when the frequency is ranging from 10 to 12.4 GHz, its RL curve is below −10 dB. These results indicate that the microwave absorbing
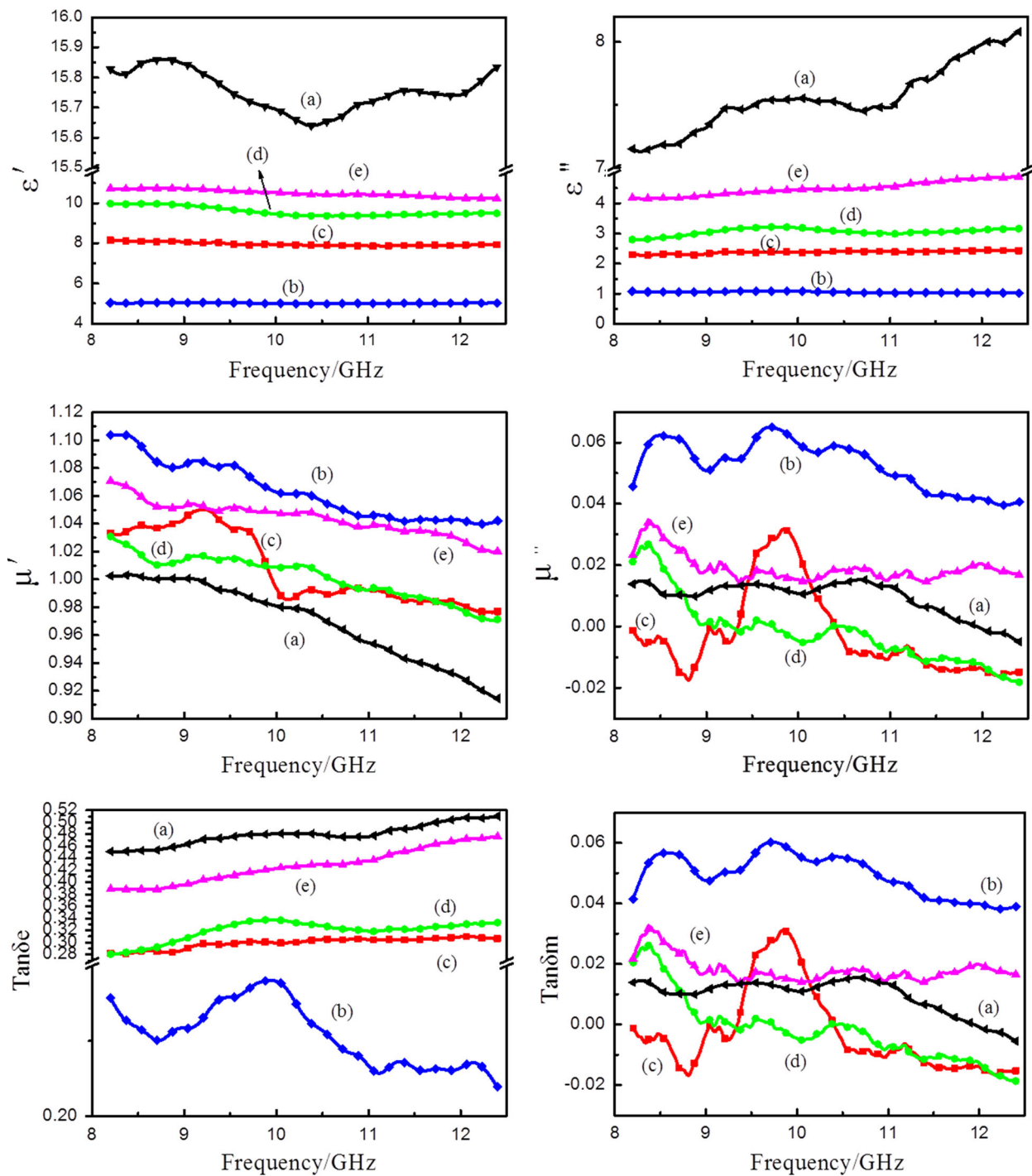
Fig. 6 Electromagnetic parameters of NanoG (*a*) NiFe$_2$O$_4$ (*b*) PANI (*c*) PANI/NanoG (*d*) and PANI/NiFe$_2$O$_4$/NanoG (*e*)

properties of PANI/NiFe$_2$O$_4$/NanoG were greatly improved compared with the other four materials. Meanwhile, the frequency band of PANI/NiFe$_2$O$_4$/NanoG is wider. This is due mainly to the addition of magnetic property by NiFe$_2$O$_4$, making the ternary composite has better electromagnetic matching than these materials.

As the matching thickness of the absorber is one of the crucial parameters which could determine the incident impedance, it is necessary to explore the influence of thickness on the absorption properties in detail. The simulated RL curves of PANI/NiFe$_2$O$_4$/NanoG at different thicknesses are shown in Fig. 8. It is obvious that the peak of RL moves toward the lower frequency region with the thickness increasing, and a maximum peak value can be observed at a certain thickness, which may be explained by the quarter-wavelength model. When the thickness is 1.5 mm, the
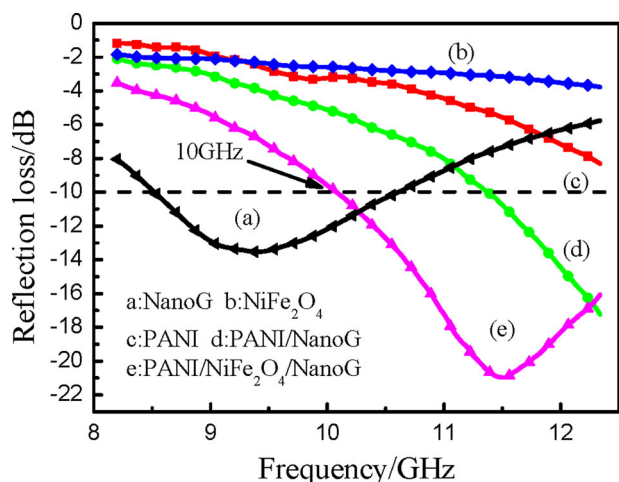
Fig. 7 RL curves of NanoG (*a*) NiFe$_2$O$_4$ (*b*) PANI (*c*) PANI/NanoG (*d*) and PANI/NiFe$_2$O$_4$/NanoG (*e*)
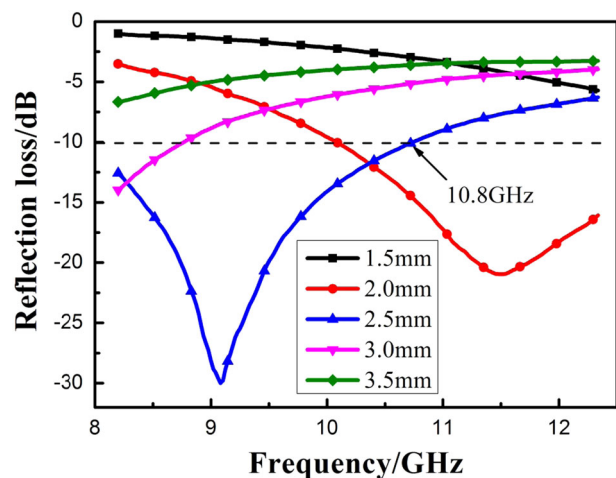

Fig. 8 RL curves of PANI/NiFe$_2$O$_4$/NanoG at different thicknesses

RL value is less than −5 dB. However, when the thickness increased to 2.5 mm, its RL curve is ranging from −6.3 to −30 dB, and the maximum value appeared at F = 9.1 GHz. When the frequency ranges from 8.2 to 10.8 GHz, its RL values are all more than −10 dB. Its microwave absorb-ability is better than the 2.0 mm sample, and the frequency band became wider. When the thickness reached 3.0 and 3.5 mm, its RL value is decreased with the increase of the thickness, which is less than the 2.5 mm sample. So we can draw the conclusion that the best match thickness of PANI/NiFe$_2$O$_4$/NanoG is 2.5 mm in the X band, and the RL is lower both in low and high frequency.

4 Conclusions

In summary, the PANI/NiFe$_2$O$_4$/NanoG ternary composite with perfect microwave absorption properties were prepared

by a facile two-step method. According to measurements from SEM, TEM and XRD, the NanoG is coated by NiFe$_2$O$_4$ layer after sol-gel reaction, and NiFe$_2$O$_4$/NanoG is uniformly wrapped by PANI after in situ polymerization. Measurement of TGA shows that the thermal stability of PANI is improved by the addition of NanoG. The four-point-probe and VSM test suggest that the PANI/NiFe$_2$O$_4$/NanoG's conductivity and Ms value are 0.2 S/cm and 10 emu/g, respectively. Above all, the PANI/NiFe$_2$O$_4$/NanoG has excellent microwave absorbing properties, its RL value can reach up to −21 dB when its thickness is 2.0 mm and −30 dB when its thickness is 2.5 mm. Based from the above results, the PANI/NiFe$_2$O$_4$/NanoG composite is therefore an excellent candidate for application as a microwave absorber.

Compliance with ethical standards

References

1. Khairy M (2014) Synth Met 189:34–41
2. Wang T, Wang H, Chi X, Li R, Wang J (2014) Carbon N Y 74:312–318
3. Yuan CL, Hong YS (2010) J Mater Sci 45:3470–3476
4. Wen QL, Zhou WC, Su JB, Qing YC, Liu F, Zhu DG (2016) J Alloys Compd 666:359–365.
5. Xie ZL, Huang X, Titirici MM, Taubert A (2014) RSC Adv 4:37423–37430
6. Xu J, Wang K, Zu S, Han B, Wei Z (2010) ACS Nano 4:5019
7. Cao M, Song W, Hou Z, Wen B, Yuan J (2010) Carbon N Y 48:788–796
8. Qing YC, Wen QL, Luo F, Zhou WC, Zhu DM (2016) J Mater Chem C 4.2:371–375
9. Maqsood A, Khan K (2011) J Alloys Compd 509:3393–3397
10. Chen XL, Wang XW, Li LD, Qi SH (2016) J Mater Sci Mater Electron 27:5607–5612
11. Yang J, Zhou YZ, Sun L, Zhao N, Zang CL, Cheng XN (2012) Appl Surf Sci 258:5056–5060
12. Qing YC, Ming DD, Zhou YY, Luo F, Zhou WC (2015) Carbon N Y 86:98–107
13. Jiang J, Li LC, Xu F (2007) Mater Sci Eng A 456:300–304
14. Li YB, Yi R, Yan A, Deng LW, Zhou KC, Liu XH (2009) Solid State Sci 11:1319–1324
15. Duan YP, Liu Z, Jing H, Zhang YH, Li SQ (2012) J Mater Chem 22:18291–18299
16. Moucka R, Mravcakova M, Vilcakova J, Omastova M, Saha P (2011) Mater Des 32:2006–2011
17. Chen XC, Hou CY, Zhang QH, Li YG, Wang HZ (2012) Mater Sci Eng, B 177:1067–1072
18. Kassaee MZ, Motamedi E, Majdi M (2011) Chem Eng J 172:540–549
19. Bai X, Zhai YH, Zhang Y (2011) J Phys Chem C 115:11673–11677
20. Wang Y, Huang Y, Wang QF, He Q, Zong M (2013) J Sol Gel Sci Technol 67:344–350
21. Paek SM, Yoo EJ, Honma I (2009) Nano Lett 9:72–75
22. Zhang JT, Zhao XS (2012) J Phys Chem C 116:5420
23. Li JH, Da HF, Liu Q, Liu SS (2006) Mater Lett 29–30:3927–3930